Rapid Communications

From topologically protected coherent perfect reflection to bound states in the continuum

Shiwei Dai,[1] Liang Liu,[1] Dezhuan Han,[1,*] and Jian Zi[2,†]

[1]*Department of Applied Physics, Chongqing University, Chongqing 401331, China*

[2]*Department of Physics, Key Laboratory of Micro- and Nano-Photonic Structures (MOE), and State Key Laboratory of Surface Physics, Fudan University, Shanghai 200433, China*

A mechanism for perfect reflection is proposed for the dielectric medium beyond the total internal reflection and band gaps. It arises from the coherence of multiple propagating modes, and can be determined by the topological vortex of a transmission coefficient with a nonzero winding number in parameter space. Based on the coherent perfect reflection, a generalized waveguide condition is derived analytically. In a photonic crystal slab, the modes that satisfy this condition are precisely bound states in the continuum. Our findings may have many potential applications in guided-wave optics.

Guiding light is significant in classical and modern optics. As the basis of guided-wave optics, the total internal reflection plays a key role in modern optical fiber communication networks [1]. Complete reflection can also be achieved by the interference of light reflected from the upper and lower boundaries of a thin film. If a single boundary is considered, photonic band gaps can provide another mechanism for guiding light in addition to index guiding [2–4]. Band-gap confinement is extensively adopted in the miniaturization and integration of optical components [5]. Both of the above mechanisms require an essential element, a mirror to reflect and guide light. With the mirror, the corresponding radiation channels can be closed. Recently, a topologically nontrivial mirror has received considerable interest in photonic systems [6]. If a topological phase transition takes place, namely, that the topology of the frequency band is different across an interface, edge states are guaranteed to exist within the bulk gap, which leads to the robust unidirectional propagation of light and other remarkable phenomena [7–16].

Here, we propose a mechanism for designing the mirror, called coherent perfect reflection (CPR). Compared to the total internal reflection and band gap working for an individual ray or Bloch mode, this CPR comes from the coherence of propagating modes supported in the photonic structure. It is demonstrated that a transmission vortex can exist if the coefficient ratio of the propagating modes is chosen properly. This effect is topological since the complex transmission coefficient has a nonzero winding number in parameter space. In contrast to a topologically nontrivial mirror [6] with working frequencies in the bulk band gaps, the CPR has its working frequencies in the passing bands. With this type of mirror, the conventional waveguide condition (total internal reflection and resonance condition) for the planar dielectric waveguide can be generalized to the CPR and resonance conditions. In a photonic crystal (PC) slab, the topological singularity of the

transmission coefficient can be maintained while light travels along the waveguide if the mode satisfies the generalized waveguide condition.

This generalized waveguide condition can be associated with the well-known bound states in the continuum (BICs). As a type of bound state embedded in the continuum, the BIC was first proposed in a quantum system [17] and later revealed to be a general wave phenomenon [18]. It has been extended in various physical systems such as photonics [19–26], acoustics [27,28], and water waves [29,30]. The infinitely high-quality factor of BICs renders many applications possible [31–34]. Recently, the topological nature of BICs in PC slabs has been demonstrated, which corresponds to vortex centers in the polarization directions of far-field radiation [22]. The robust existence of BICs in periodic structures is therefore connected to topological physical phenomena beyond the band-structure analysis [22,26,28,35]. Here, we demonstrate that the BICs can be naturally obtained as a result of the generalized waveguide condition by combining the proposed CPR and resonance conditions.

The mechanism for the CPR is presented in Fig. 1. Total internal reflection takes place outside the light cone as sketched in Figs. 1(a) and 1(c). The corresponding incident angle has to exceed the critical angle and is usually large if the relative refractive index is not too high. Within the light cone, the propagating modes will transmit through the interface. However, there may exist multiple modes sharing the same parallel component of momentum as shown in Figs. 1(b) and 1(d). For an incident wave indexed by n, the corresponding complex coefficients of transmission $t^{(n)}$ are nonzero. If there are N modes in total impinging on the interface, intriguingly, there is a special kind of perfect reflection named CPR, coming from the destructive interference of these modes. The CPR condition is such that

$$\sum t^{(n)} = 0. \tag{1}$$

The cancellation of all the complex coefficients can be sketched in the complex plane, shown by a phasor diagram in the inset of Fig. 1(b). This condition can be reached by controlling the

---

*dzhan@cqu.edu.cn

†jzi@fudan.edu.cn
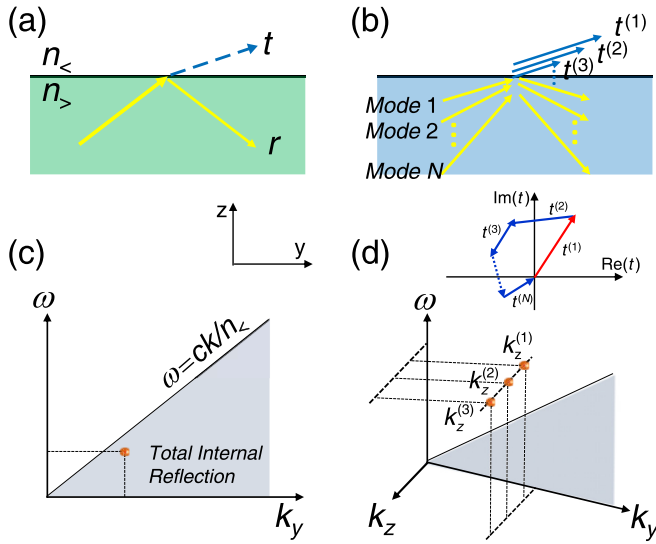
FIG. 1. (a) Schematic of total internal reflection. It occurs below the light line $\omega = ck/n_<$ as shown in (c). (b) Transmission of multiple incident modes. These modes share the same parallel component of wave vector k_y while possessing a different normal component k_z inside the light cone, as shown in (d).

relative ratio of complex amplitudes between these modes. It offers a mechanism for designing a mirror to reflect light inside the light cone if there are multiple propagating modes sharing the same parallel component of momentum.

With this type of mirror, light can be further guided based on the CPR mechanism. In Fig. 2, a special waveguide that supports multiple propagating modes is considered. a_n and r_n are the complex coefficients of the incident and reflected waves for the nth mode. Assuming that the CPR condition Eq. (1) is satisfied for the upper interface with a properly chosen incidence $(a_1, a_2, \ldots)$, the reflection coefficients $(r_1, r_2, \ldots)$, however, will become the corresponding incidence for the lower interface. The CPR condition can be maintained for the lower interface as long as

$$r_n/a_n = \text{const} \quad \text{for arbitrary } n. \tag{2}$$
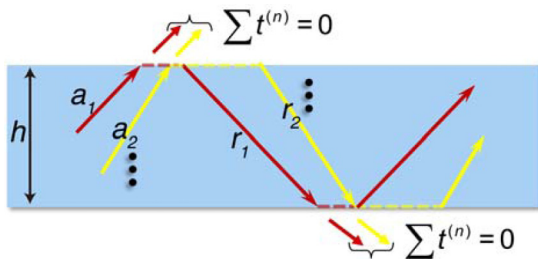
FIG. 2. A waveguide mode based on coherent perfect reflection (CPR). The condition of CPR can be maintained if the relative ratios of propagating modes are kept the same at the upper and lower interfaces when the light bounces back and forth in the waveguide. A ray model is sketched and the phase shift is indicated by an additional distance (dashed line).

In other words, the relative ratio of these modes should be preserved after a bounce. In fact, only a phase factor can exist since these modes are totally reflected. In guided-wave optics, the resonance condition is another essential point in addition to the total internal reflection [36]. This condition can also be extended for multiple rays of light. At the interface, each reflection is accompanied by a phase shift $\varphi_r^{(n)}$ for the nth propagating mode. The round-trip phase shift of each propagating mode should be an integer multiple of 2π, and the generalized resonance condition is

$$k_z^{(n)} h + \varphi_r^{(n)} = m^{(n)} \pi, \tag{3}$$

where h is the thickness of the waveguide, and $m^{(n)}$ is an integer. Equations (1)–(3) can be treated as the generalized waveguide condition for this special waveguide. This generalized condition gives the waveguide modes inside the light cone, which are BICs precisely. Combining these three equations we have $r_n/a_n = \pm 1$ for the symmetric waveguide. The positive and negative signs correspond to the even and odd symmetries of the waveguide mode.

To demonstrate the CPR, we take a one-dimensional (1D) PC as example. This PC is periodic in the y direction with a period a and uniform in the x direction, as schematically shown in Fig. 3(a). The alternating dielectric layers have a thickness d_1 and d_2, and permittivity ε_1 and ε_2, respectively. The dielectric constant of the background medium is set as ε_b. Transverse electric (TE) waves are considered without loss of generality. The dispersion relation can relate the frequency ω, the parallel component of the wave vector, and the Bloch wave vector (k_z and q), given in the Supplemental Material [37].

The complex band structures for the TE waves are shown in Fig. 3(b). Here, the parameters are chosen as $\varepsilon_1 = 1$, $\varepsilon_2 = 4.9$, $d_1 = d_2 = 0.5a$, and $q = 0.6\pi/a$. In addition to the normal dispersion for extended states (red) with $k_z^2 > 0$, the evanescent states (blue) with $k_z^2 < 0$ are also shown. These evanescent modes will decay (or grow) along the z direction, and cannot be neglected in the boundary conditions at the PC interface. Note that for a fixed frequency ω, there always exist a finite number of propagating modes (red) while an infinite number of evanescent modes (blue) as the imaginary k_z goes to infinity.

Considering a series of modes in the PC impinging on the PC interface, $(a_1, a_2, \ldots)$ are the complex coefficients for the incident waves with a fixed frequency ω and Bloch wave vector q. The electromagnetic field can be written as the superposition of all the propagating and evanescent modes. In region I shown in Fig. 3(a), one has

$$E_x^{\text{I}}(y, z) = \sum_{n=1}^{\infty} \left(a_n e^{ik_z^{(n)} z} + r_n e^{-ik_z^{(n)} z} \right) u_q^{(n)}(y) e^{iqy}, \tag{4}$$

where r_n is the complex coefficient of the reflected waves. $u_q^{(n)}(y)$ is the periodic-in-cell part of the Bloch wave function for the nth state.

In region II, similarly we have

$$E_x^{\text{II}}(y, z) = \sum_{m=-\infty}^{\infty} t_m e^{i(k_{y,m} y + k_{z,m} z)}, \tag{5}$$

where $k_{y,m} = q + 2\pi m/a$, $q = \sqrt{\varepsilon_b} k_0 \sin\theta$, and $k_{z,m} = \sqrt{\varepsilon_b k_0^2 - k_{y,m}^2}$. θ is the refraction angle. t_m is the complex co-
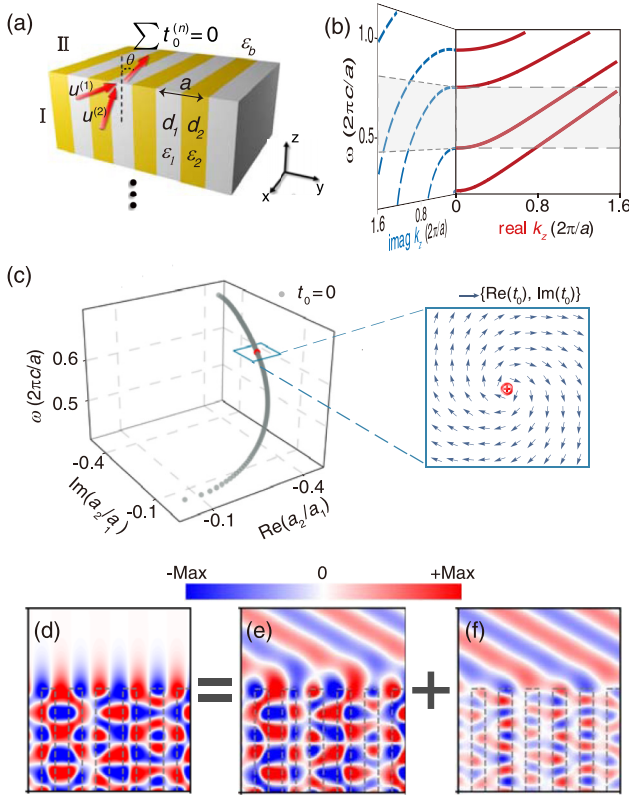
FIG. 3. Topologically protected coherent perfect reflection for a truncated photonic crystal. (a) Schematic of a semi-infinite 1D PC truncated at the $z = 0$ plane. (b) Complex band structure for a fixed Bloch wave vector q. The extended and evanescent modes are shown by the red and blue dashed lines, respectively. In the region marked in gray, there exist only two propagating modes ($u^{(1)}$ and $u^{(2)}$), while an infinite number of evanescent modes if the imaginary k_z goes to infinity. (c) Coherent perfect reflection in the parameter space [$\mathrm{Re}(a_2/a_1)$, $\mathrm{Im}(a_2/a_1)$] as a function of ω. In the box enclosing the red dot, the vector fields of {$\mathrm{Re}(t_0)$, $\mathrm{Im}(t_0)$} are shown by the arrows in the inset of (c). (d)–(f) Field profiles of $\mathrm{Re}(E_x)$ at $\omega = 1.2(\pi c/a)$. (d) is the superposition of (e) and (f), where the transmission cancels out exactly and forms coherent perfect reflection. (e) and (f) correspond to the single mode incidence with only the mode $u^{(1)}$ and $u^{(2)}$. Here, the parameters are chosen as $d_1 = d_2 = 0.5a$, $\varepsilon_1 = \varepsilon_b = 1$, $\varepsilon_2 = 4.9$, $q = 0.6\pi/a$.

efficient of total transmission for the mth diffraction order. Note that in Eq. (1), $t^{(n)}$ comes from a single channel with the incidence $a_n \neq 0$ and $a_{n'\neq n} = 0$ for all the n'th mode. Therefore, the total transmission t_m is the summation of $t_m^{(n)}$ contributed from all the individual channels n. At the interface, the boundary conditions (continuity of tangential E and H fields) should be satisfied. Including the evanescent mode near the PC interface will naturally give the additional boundary conditions in the Maxwell equations [38,39]. These boundary conditions can be rewritten by applying a Fourier transform [40].

We first consider the simplest case of semi-infinite PC truncated at a plane of $z = 0$. All the evanescent modes that increase away from the interface should be excluded. Therefore, the incidence will be $(a_1, a_2, \ldots, a_L)$ and $a_{n>L} = 0$

if the number of propagating modes is L in total and all the other modes are evanescent. In contrast, the evanescent modes can appear in the reflection and all r_n are allowed in principle. With the boundary condition, the relation between the coefficients (a_n, r_n, t_m) can be derived. The reflection and transmission properties of this semi-infinite PC are determined by the above complex coefficients [37]. The CPR condition for the truncated 1D PCs is simply that $t_m = 0$ for all the diffraction channels inside the light cone.

If the frequency ω lies in the gray region shown in Fig. 3(b), there are only two propagating modes ($a_n = 0$ for $n > 2$) in the PC, namely, $u^{(1)}$ with a smaller k_z and $u^{(2)}$ with a larger k_z. Furthermore, there might be leaky channels to the free space for the diffraction order with $m \neq 0$. Here, we focus on the case where there is only zeroth-order transmission (t_0), and all other diffraction channels for $m \neq 0$ are closed since the corresponding transmitted evanescent waves will not give rise to a leakage of energy. This theory can be directly generalized to a case with high-order diffraction channels. In Fig. 3(c), a set of points satisfying the CPR condition ($t_0 = 0$) are exhibited in the parameter space [$\mathrm{Re}(a_2/a_1)$, $\mathrm{Im}(a_2/a_1)$] as a function of ω. In general, t_0 is a complex function and the CPR corresponds to the node of this complex function. In the inset of Fig. 3(c), a two-dimensional (2D) vector field {$\mathrm{Re}(t_0)$, $\mathrm{Im}(t_0)$} is introduced to represent the complex t_0. Interestingly, the CPR is the center of the vortex of transmission shown in the box (red dot). The corresponding winding number around the CPR point is $+1$, manifesting that the effect of CPR is topological in nature. And as the frequency varies, the locus of this topological singularity in the complex plane [$\mathrm{Re}(a_2/a_1)$, $\mathrm{Im}(a_2/a_1)$] also changes and forms a path of CPR as indicated in Fig. 3(c). Therefore, the CPR can be precisely achieved by controlling the ratio of the complex coefficient of the two propagating modes.

The spatial field profiles of $\mathrm{Re}(E_x)$ at $\omega = 1.2(\pi c/a)$ corresponding to the red dot in Fig. 3(c) are shown in Fig. 3(d). In simulations, the two Bloch waves in the semi-infinite PC can be reproduced by periodic point sources [37]. We can thus separate the two Bloch waves for the incidence. Figures 3(e) and 3(f) correspond respectively to the single mode incidence with only the mode $u^{(1)}$ and $u^{(2)}$ impinging on the PC interface. When the ratio of these two incidence waves, namely, a_1 and a_2, are set to match the CPR condition, the outgoing waves in Figs. 3(e) and 3(f) will have the same magnitude but opposite phase. Hence, the superposition of Figs. 3(e) and 3(f) leads to an efficient suppression of transmission and forms the CPR shown in Fig. 3(d). These simulated results confirm our theoretical prediction.

Distinct from the semi-infinite PC, a PC slab with a finite thickness can support evanescent waves with both positive and negative attenuation. The CPR condition at two interfaces requires that the relative phase and amplitude of all the modes remain the same after a bounce. Therefore, the previous condition $a_n = 0$ ($n > L$ for all the evanescent modes) in the boundary conditions for the truncated PC should be replaced by Eq. (2) for the PC slab. Equations (1) and (2), and the resonance condition Eq. (3) for the propagating modes ($n \leqslant L$), are thus forming the generalized waveguide condition. Some isolated states, such as states C and D satisfying the generalized waveguide condition, are marked in Fig. 4(a),
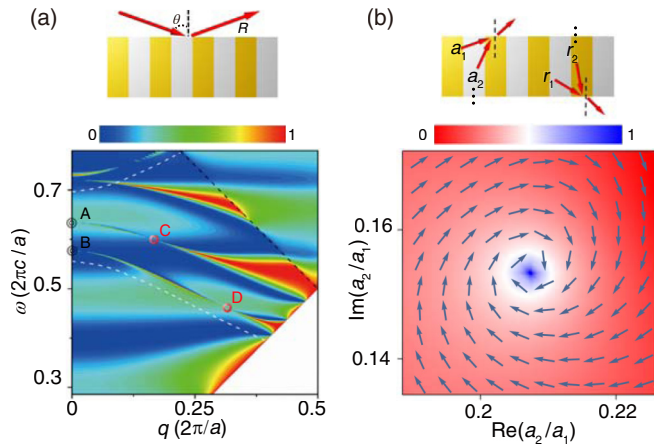
FIG. 4. Characterization of bound states in the continuum. Two schemes are considered: (a) a PC slab illuminated by an external plane wave, and (b) multiple Bloch modes incident inside a PC slab. The simulated reflection spectra are shown in (a). The theoretical results calculated by the generalized waveguide conditions are marked by A, B and C, D, corresponding to the at-Γ and off-Γ BICs, respectively. The region with only one leaky channel and two propagating modes in the PC is enclosed by the dotted black and white lines. In (b), the vortex of transmission t_0 is shown for state D under the condition that $r_1/a_1 = r_2/a_2$ [Eq. (2) applied only for the two propagating modes]. The ratio of evanescent waves exemplified by r_3/a_3 is plotted in the color scale. Two conditions for the BICs should be satisfied: vortex of transmission and $r_n/a_n = 1$ for the evanescent modes. Here, the thicknesses of the slab is set as $1.4a$, and other parameters are the same as those in Fig. 3(a).

indicating that the CPR condition can be strictly maintained for each bounce and the leaky channels are closed for this mode. These nonradiating modes can also be verified by the reflection spectra of the PC slab. If this slab is illuminated by an external plane wave, a reflection peak will appear if a resonant mode exists. In the PC slabs, the BICs have been theoretically identified and experimentally observed on the dispersion curves of guided resonant modes since they cannot be excited by the external waves [19–24]. In Fig. 4(a), the reflection spectra as a function of q and ω are shown in the color scale. The reflection peaks disappear at points A, B, C, and D, agreeing well with the theoretically predicted results.

It should be mentioned that $u^{(1)}$ is an antisymmetric mode at the Γ point. Its corresponding zeroth-order Fourier component $\tilde{u}_{q,0}^{(1)} = \frac{1}{a}\int_0^a u_q^{(1)}(y)dy = 0$, therefore all the coefficients a_n and r_n for $n > 1$ will vanish following from Eqs. (S2) and (S3) [37]. This antisymmetric mode at the Γ point decouples from the external radiation naturally due to the symmetry property, and forms another kind of symmetry-protected BIC rather than a CPR-based BIC.

To investigate the topological properties of these special waveguide modes residing inside the light cone, the vector field of $\{\mathrm{Re}(t_0), \mathrm{Im}(t_0)\}$ in the complex plane of $[\mathrm{Re}(a_2/a_1), \mathrm{Im}(a_2/a_1)]$ is plotted in Fig. 4(b) for state D in Fig. 4(a). In contrast to the case of a semi-infinite PC in Fig. 3(a) where we set $a_n = 0$ ($n > 2$ for all the evanescent modes), here we fix the ratio of the propagating modes $r_1/a_1 = r_2/a_2$ and release the condition for the evanescent waves. The ratio of coefficients r_n/a_n ($n > 2$) for the evanescent waves can be solved from the boundary conditions. As an example, $|r_3|/|a_3|$ is plotted in the color scale. The bound state D takes place at the vortex center of t_0 as expected. Moreover, $|r_3|/|a_3| = 1$ is satisfied at the vortex center, which will give rise to a BIC exactly. The CPR condition can be maintained since the relative phase and magnitude of all the coefficients $(a_1, a_2, \ldots)$ and $(r_1, r_2, \ldots)$ are preserved for any bounce at the PC interface.

In conclusion, we have demonstrated a different kind of perfect reflection, which is associated with a topological vortex of transmission. This mechanism is based on the coherence of multiple modes sharing the same parallel component of momentum, and can work for any frequency and wave vector. Based on the CPR, a generalized waveguide condition is derived. Through the generalized conditions, the special waveguide modes in the PC slab, or BICs, can be fixed analytically. This perfect reflection therefore offers a scheme to design the mirror and is of both theoretical and practical interest in guided-wave optics.

[1] B. E. A. Saleh and M. C. Teich, *Fundamentals of Photonics* (Wiley, New York, 1991).

[2] E. Yablonovitch, Phys. Rev. Lett. **58**, 2059 (1987).

[3] S. John, Phys. Rev. Lett. **58**, 2486 (1987).

[4] J. D. Joannopoulos, S. G. Johnson, J. N. Winn, and R. D. Meade, *Photonic Crystals: Molding the Flow of Light*, 2nd ed. (Princeton University Press, Princeton, NJ, 2008).

[5] T. Baba, Nat. Photonics. **2**, 465 (2008).

[6] L. Lu, J. D. Joannopoulos, and M. Soljačić, Nat. Photonics. **8**, 821 (2014).

[7] F. D. M. Haldane and S. Raghu, Phys. Rev. Lett. **100**, 013904 (2008).

[8] Z. Wang, Y. D. Chong, J. D. Joannopoulos, and M. Soljačić, Phys. Rev. Lett. **100**, 013905 (2008).

[9] K. Fang, Z. Yu, and S. Fan, Nat. Photonics **6**, 782 (2012).

[10] M. C. Rechtsman, J. M. Zeuner, Y. Plotnik, Y. Lumer, D. Podolsky, F. Dreisow, S. Nolte, M. Segev, and A. Szameit, Nature (London) **496**, 196 (2013).

[11] M. Hafezi, S. Mittal, J. Fan, A. Migdall, and J. M. Taylor, Nat. Photonics **7**, 1001 (2013).

[12] W.-J. Chen, S.-J. Jiang, X.-D. Chen, B. Zhu, L. Zhou, J.-W. Dong, and C. T. Chan, Nat. Commun. **5**, 5782 (2014).

[13] L.-H. Wu and X. Hu, Phys. Rev. Lett. **114**, 223901 (2015).

[14] X. Cheng, C. Jouvaud, X. Ni, S. H. Mousavi, A. Z. Genack, and A. B. Khanikaev, Nat. Mater. **15**, 542 (2016).

[15] C. He, X.-C. Sun, X.-P. Liu, M.-H. Lu, Y. Chen, L. Feng, and Y.-F. Chen, Proc. Natl. Acad. Sci. USA **113**, 4924 (2016).

[16] X. Wu, Y. Meng, J. Tian, Y. Huang, H. Xiang, D. Z. Han, and W. Wen, Nat. Commun. **8**, 1304 (2017).

[17] J. von Neuman and E. Wigner, Phys. Z. **30**, 467 (1929).

[18] C. W. Hsu, B. Zhen, A. D. Stone, J. D. Joannopoulos, and M. Soljačić, Nat. Rev. Mater. **1**, 16048 (2016).

[19] D. C. Marinica, A. G. Borisov, and S. V. Shabanov, Phys. Rev. Lett. **100**, 183902 (2008).

[20] C. W. Hsu, B. Zhen, J. Lee, S.-L. Chua, S. G. Johnson, J. D. Joannopoulos, and M. Soljačić, Nature (London) **499**, 188 (2013).

[21] Y. Yang, C. Peng, Y. Liang, Z. Li, and S. Noda, Phys. Rev. Lett. **113**, 037401 (2014).

[22] B. Zhen, C. W. Hsu, L. Lu, A. D. Stone, and M. Soljačić, Phys. Rev. Lett. **113**, 257401 (2014).

[23] X. Gao, C. W. Hsu, B. Zhen, X. Lin, J. D. Joannopoulos, M. Soljačić, and H. Chen, Sci. Rep. **6**, 31908 (2016).

[24] Y. Zhang, A. Chen, W. Liu, C. W. Hsu, B. Wang, F. Guan, X. Liu, L. Shi, L. Lu, and J. Zi, Phys. Rev. Lett. **120**, 186103 (2018).

[25] S. Weimann, Y. Xu, R. Keil, A. E. Miroshnichenko, A. Tünnermann, S. Nolte, A. A. Sukhorukov, A. Szameit, and Y. S. Kivshar, Phys. Rev. Lett. **111**, 240403 (2013).

[26] E. N. Bulgakov and D. N. Maksimov, Phys. Rev. Lett. **118**, 267401 (2017).

[27] N. A. Cumpsty and D. S. Whitehead, J. Sound Vib. **18**, 353 (1971).

[28] Y. X. Xiao, G. Ma, Z. Q. Zhang, and C. T. Chan, Phys. Rev. Lett. **118**, 166803 (2017).

[29] R. Porter and D. V. Evans, Wave Motion **43**, 29 (2005).

[30] C. M. Linton and P. McIver, Wave Motion **45**, 16 (2007).

[31] K. Hirose, Y. Liang, Y. Kurosaka, A. Watanabe, T. Sugiyama, and S. Noda, Nat. Photonics **8**, 406 (2014).

[32] A. Kodigala, T. Lepetit, Q. Gu, B. Bahari, Y. Fainman, and B. Kanté, Nature (London) **541**, 196 (2017).

[33] A. A. Yanik, A. E. Cetin, M. Huang, A. Artar, S. H. Mousavi, A. Khanikaev, J. H. Connor, G. Shvets, and H. Altug, Proc. Natl. Acad. Sci. USA **108**, 11784 (2011).

[34] J. M. Foley, S. M. Young, and J. D. Phillips, Phys. Rev. B **89**, 165111 (2014).

[35] Y. Guo, M. Xiao, and S. Fan, Phys. Rev. Lett. **119**, 167401 (2017).

[36] A. Yariv and P. Yeh, *Photonics: Optical Electronics in Modern Communications* (Oxford University Press, New York, 2006).

[37] See Supplemental Material at http://link.aps.org/supplemental/10.1103/PhysRevB.98.081405 for the dispersion relation, additional boundary condition, incidence of a single propagating mode, relation between the CPR and topological vortices, and perturbation of CPR.

[38] C. S. Ting, M. J. Frankel, and J. L. Birman, Solid State Commun. **17**, 1285 (1975).

[39] R. L. Chern, D. Z. Han, Z. Q. Zhang, and C. T. Chan, Opt. Express **22**, 31677 (2014).

[40] P. Sheng, R. S. Stepleman, and P. N. Sanda, Phys. Rev. B **26**, 2907 (1982).